

Crystal growth of $CeMn_{0.85}Sb_2$:Absence of magnetic order of Ce-sublattice

Yong Li(李勇), Shan-Shan Miao(苗杉杉), Hai Feng(冯海), Huai-Xin Yang(杨槐馨), and You-Guo Shi(石友国)
Citation: Chin. Phys. B, 2023, 32 (**6**): 067501. DOI: 10.1088/1674-1056/acc060
Journal homepage: http://cpb.iphy.ac.cn; http://iopscience.iop.org/cpb

What follows is a list of articles you may be interested in

Prediction of $LiCrTe_2$ monolayer as a half-metallic ferromagnet with a high Curie temperature

Li-Man Xiao(肖丽蔓), Huan-Cheng Yang(杨焕成), and Zhong-Yi Lu(卢仲毅)
Chin. Phys. B, 2023, 32 (**5**): 057505. DOI: 10.1088/1674-1056/acbe2e

A spin-based magnetic scanning microscope for *in-situ* strain tuning of soft matter

Zhe Ding(丁哲), Yumeng Sun(孙豫蒙), Mengqi Wang(王孟祺), Pei Yu(余佩), Ningchong Zheng(郑宁冲), Yipeng Zang(臧一鹏), Pengfei Wang(王鹏飞), Ya Wang(王亚), Yuefeng Nie(聂越峰), Fazhan Shi(石发展), and Jiangfeng Du(杜江峰)
Chin. Phys. B, 2023, 32 (**5**): 057504. DOI: 10.1088/1674-1056/acbaee

Strong spin frustration and magnetism in kagomé antiferromagnets $LnCu_3(OH)_6Br_3$ (*Ln*=Nd, Sm, and Eu)

Jin-Qun Zhong(钟金群), Zhen-Wei Yu(余振伟), Xiao-Yu Yue(岳小宇), Yi-Yan Wang(王义炎), Hui Liang(梁慧), Yan Sun(孙燕), Dan-Dan Wu(吴丹丹), Zong-Ling Ding(丁宗玲), Jin Sun(孙进), Xue-Feng Sun(孙学峰), and Qiu-Ju Li(李秋菊)
Chin. Phys. B, 2023, 32 (**4**): 047505. DOI: 10.1088/1674-1056/acb9e8

Abnormal magnetic behavior of prussian blue analogs modified with multi-walled carbon nanotubes

Jia-Jun Mo(莫家俊), Pu-Yue Xia(夏溥越), Ji-Yu Shen(沈纪宇), Hai-Wen Chen(陈海文), Ze-Yi Lu(陆泽一), Shi-Yu Xu(徐诗语), Qing-Hang Zhang(张庆航), Yan-Fang Xia(夏艳芳), and Min Liu(刘敏)
Chin. Phys. B, 2023, 32 (**4**): 047503. DOI: 10.1088/1674-1056/ac946b

Orbital torque of Cr-induced magnetization switching in perpendicularly magnetized Pt/Co/Pt/Cr heterostructures

Hongfei Xie(谢宏斐), Yuhan Chang(常宇晗), Xi Guo(郭玺), Jianrong Zhang(张健荣), Baoshan Cui(崔宝山), Yalu Zuo(左亚路), and Li Xi(席力)
Chin. Phys. B, 2023, 32 (**3**): 037502. DOI: 10.1088/1674-1056/aca6d7

Crystal growth of $CeMn_{0.85}Sb_2$: Absence of magnetic order of Ce-sublattice

Yong Li(李勇)[1,2,3], Shan-Shan Miao(苗杉杉)[1], Hai Feng(冯海)[1,4,†], Huai-Xin Yang(杨槐馨)[1,3,‡], and You-Guo Shi(石友国)[1,2,4,§]

[1] *Beijing National Laboratory for Condensed Matter Physics and Institute of Physics, Chinese Academy of Sciences, Beijing* 100190, *China*
[2] *Center of Materials Science and Optoelectronics Engineering, University of Chinese Academy of Sciences, Beijing* 100190, *China*
[3] *School of Physical Sciences, University of Chinese Academy of Sciences, Beijing* 100190, *China*
[4] *Songshan Lake Materials Laboratory, Dongguan* 523808, *China*

(Received 7 January 2023; revised manuscript received 1 March 2023; accepted manuscript online 2 March 2023)

Single crystals of $CeMn_{0.85}Sb_2$ have been successfully synthesized by using the Bi as flux. Analysis of single crystal x-ray diffraction data confirms that $CeMn_{0.85}Sb_2$ crystallizes in the $HfCuSi_2$-type structure with the space group $P4/nmm$ (No. 129). In the case of $H \parallel c$, $CeMn_{0.85}Sb_2$ displays a robust antiferromagnetic transition at $\sim$ 160 K for Mn-sublattice, and there is no sign of magnetic order regarding Ce-sublattice. In the case of $H \perp c$, the Mn-sublattice shows signs of magnetic order at 160 K and 116 K, indicating a possible spin reorientation. There is no sign of magnetic order for the Ce-sublattice either, but, alternating current magnetic susceptibility measurements reveal a spin glass state below 18 K in the case of $H \perp c$. Isothermal magnetization curves measured below magnetic order with $H \perp c$ show saturation and even large hysteresis at 2 K, indicating the presence of a ferromagnetic component. In addition, a field-induced spin-flop transition is observed in the case of $H \perp c$, indicating a field-induced spin reorientation of Mn spins. Electrical resistivity measurements indicate a metallic nature for $CeMn_{0.85}Sb_2$ and large anisotropy which is consistent with its quasi-two-dimensional layered structure.

Keywords: $CeMn_{0.85}Sb_2$, magnetism, spin glass, layered structure, square lattice

PACS: 75.10.Nr, 75.30.Gw, 71.20.Lp **DOI:** 10.1088/1674-1056/acc060

1. Introduction

Intermetallic compounds with a general formula ATX_2 (A = Ca, Sr, Ba, or a rare earth element; T = a transition metal element; X = Sb or Bi) can host numerous exotic phenomena such as giant magnetoresistance, Dirac semimetals, Weyl semimetals, and magnetic Weyl semimetals.[1–18] Particularly, Ce-based $CeTX_2$ intermetallic compounds show Kondo behavior, magnetic orders, and superconductivity due to competition between the Ruderman–Kittle–Kasuya–Yosida (RKKY) magnetic interactions and the on-site Kondo interactions.[19–21] Interestingly, both antiferromagnetic (AFM) and ferromagnetic (FM) orders have been reported for $CeTX_2$ with different lattice parameters, indicating that the RKKY interactions are sensitive to the distance between Ce ions.[22–24] Rosa *et al.* proposed that the magnetism in this family of compounds can also be understood based on the subtle changes of c/a.[24]

When T = Mn, $AMnX_2$ intermetallic compounds distinguish themselves from the family because the Mn-sublattices generally display AFM orders with relatively high transition temperatures. For instance, compounds $AMnX_2$ (A = Ca, Sr, Ba; X = Bi, Sb) all show high-temperature (> 280 K) AFM orders for the Mn-sublattice.[1,7,18,25–27] When A is a magnetic rare-earth element, $AMnX_2$ shows successive AFM orders corresponding to both Mn and rare-earth sublattices, respectively. Examples are $EuMnSb_2$, $EuMnBi_2$, $PrMn_{0.81}Sb_2$, and $NdMn_{0.88}Sb_2$ exhibiting two AFM orders related to magnetic sublattices of rare earth and Mn sublattices, respectively.[12,28–30] Studies on $PrMn_{0.81}Sb_2$ suggested that the AFM orders for Mn and Pr-sublattices are in competition.[28] The magnetic structures of Mn or rare earth sublattices would also influence the transport properties dominated by the Sb or Bi square lattice.[31–34]

Compounds $CeTX_2$, containing only magnetic Ce-sublattice, generally show AFM or FM order with different lattice parameters.[22–24] However, $CeMnX_2$ compounds with both Ce and Mn-sublattices have not been well studied. A previous study on a polycrystalline sample of $CeMn_{1-\delta}Sb_2$ indicated magnetic orders for both Mn and Ce-sublattices.[35] In this work, we want to investigate the detailed magnetic and electrical properties of $CeMnSb_2$ based on the single crystals. By using the Bi flux, we successfully synthesize high-quality $CeMnSb_2$ single crystals and study their detailed anisotropic magnetism and resistivity. Our studies of $CeMnSb_2$ find an AFM order for the Mn-sublattice (160 K), but no sign of mag-

†Corresponding author. E-mail: hai.feng@iphy.ac.cn
‡Corresponding author. E-mail: hxyang@iphy.ac.cn
§Corresponding author. E-mail: ygshi@iphy.ac.cn

© 2023 Chinese Physical Society and IOP Publishing Ltd

netic order for the Ce-sublattice.

2. Experimental details

Single crystals of $CeMnSb_2$ were grown from Bi flux with starting elements of Ce (ingot, 99.9%, Purui Advanced Material Technology Co. Ltd., Beijing, China), Mn (pieces, 999.98%, Alfa Aesar), Sb (pills, 99.999%, Alfa Aesar), and Bi (pills, 99.999%, Alfa Aesar) with a molar ratio of 1:1:2:6. The mixture was placed in an alumina crucible which was then sealed in a quartz tube. The sealed tube was heated up to 1323 K in 10 h and then dwelt for 24 h before cooling down to 923 K at a cooling rate of 2 K/h. The excess Bi flux was removed by centrifugation at 923 K, and shiny plate-like single crystals with a typical size of 10 mm × 10 mm × 3 mm were obtained (see the inset in Fig. 1(b)). The crystals were stable in the air.

Single-crystal x-ray diffraction (SCXRD) data were collected on a Bruker D8 VENTURE PHOTON II diffractometer with Mo $K\alpha$ ($\lambda = 0.71073$ Å) radiation. Unit cell refinement and data merging were done with the SAINT program, and an absorption correction was applied using the multi-scan. Structural solutions were obtained by intrinsic phasing methods using the program APEX3, and the final refinement was completed by a full-matrix least-squares method on F^2 using the SHELXL-2016/6 programs.[36,37] Powder x-ray diffraction (PXRD) was performed in Rigaku SmartLab 9 kW (Cu $K\alpha$) and structure refinement was performed with the program package GSAS-II suite.[38]

Magnetic properties were measured in a magnetic properties measurement system (MPMS-III, Quantum Design Inc.). Magnetic susceptibility (χ) was measured at temperatures between 2 K to 300 K under varied magnetic fields (H) with field-cooling (FC) and zero-field-cooling (ZFC) conditions. Isothermal magnetizations were measured between magnetic fields of −70 kOe to 70 kOe. The alternating current (AC) magnetic susceptibility was measured at several frequencies between 2 K and 80 K in the MPMS with an excitation field $H = 3$ Oe. The C_p was measured by a thermal-relaxation method in a physical property measurement system (PPMS-9T, Quantum Design Inc.). The samples were thermally connected to the holder stage with Apiezon N grease. Electrical resistivity (ρ) and magnetoresistance were measured in the PPMS-9T using the standard four-probe method.

3. Results and discussion

3.1. Crystal structure

Analysis of the SCXRD data measured at room temperature indicates that $CeMnSb_2$ crystallizes in the $HfCuSi_2$-type structure with the tetragonal space group $P4/nmm$ (No. 129), which is as same as other similar $AMnSb_2$ (A = La, Yb, Pr, Nd) compounds.[28,30,39] In this structure, Ce occupies the crystallographic $2c$ (1/4,1/4,z) site, Mn occupies the $2b$ (3/4,1/4,0) site, and Sb occupies the $2a$ (3/4,1/4,0) and $2c$ (1/4,1/4,2/3) sites. The refined cell parameters are $a = 4.3655(4)$ Å and $c = 10.7662(1)$ Å, which are comparable to those reported for the polycrystalline sample.[35] During the refinement, we find a considerable amount of Mn deficiency, and the final refined composition is $CeMn_{0.85}Sb_2$. The goodness of fit for the final refinement is 1.119. Detailed crystallographic information is shown in Table 1. Refined atomic positions and displacement parameters are summarized in the crystallographic information file (Cif) attached as the supplemental materials.[40] The Mn deficiency has also been reported in previous polycrystalline work. It should be noted that deficiency at the transition metal site is a common phenomenon in this family, as observed in $AMn_{1-\delta}Sb_2$ (A = La–Sm), $CeZn_{1-\delta}Sb_2$, $CeAu_{1-\delta}Bi_2$, $CeNi_{1-\delta}Bi_2$, and $CeAu_{1-\delta}Sb_2$.[35,41–45] This deficiency can be explained using the Zintl concept, the electron partition for $ATSb_2$ can be simplified as $A^{2+}T^{2+}Sb^{3-}Sb^{1-}$.[45] Thus, it becomes electron-rich when A is a trivalent ion and then a deficiency in the T site can compensate for it. This oversimplified scenario can be supported by the stochiometric compositions when A is a divalent ion, such as $BaMnSb_2$,[27] $CaMnSb_2$,[3] $EuMnSb_2$,[41] and $YbMnSb_2$.[9,45]

Table 1. Crystallographic data of $CeMn_{0.85}Sb_2$.

Empirical formula	$CeMn_{0.85}Sb_2$
Formula weight	430.33 g/mol
Temperature	299(2) K
Wavelength	0.71073 Å
Crystal system	tetragonal
Space group	$P4/nmm$
Cell parameters	$a = b = 4.3690(8)$ Å
	$c = 10.799(3)$ Å
	$\alpha = \beta = \gamma = 90^\circ$
Cell volumes	206.13(9) Å^3
Z	2
Density	6.933 g/cm^3
F (000)	363
hkl range	$-6 < h < 7$, $-7 < k < 7$, $-17 < l < 18$
Θ_{min}, Θ_{max}	3.7738, 36.4128
Linear absorption coefficient	26.108 mm^{-1}
No. of reflections	4250
No. of independent reflections	350
No. of observed reflections	350
R factors	$R_1 = 0.019$, $wR_2 = 0.051$
Goodness of fit	1.119
Weighting scheme	$w = 1/[\sigma^2(F_o^2) + (0.0141P)^2 + 2.382P]$
	where $P = (F_o^2 + 2F_c^2)/3$
Refinement software	SHELXL-2016/6

The crystal structure obtained from the refinement is illustrated in Fig. 1(a). Their structure can be understood from

the stacking arrangement of CeSb–Mn–CeSb–Sb, for which two-dimensional square nets are formed by Mn and Sb1. The distance between Ce ions is 4.366 Å in the *ab* plane, which is comparable to 4.363 Å in $CeAgSb_2$. Figure 1(b) shows a typical out-of-plane x-ray diffraction pattern of the obtained sample. The major peaks are (00*l*), indicating that the surface of the sample is (00*l*). To further check the purity, single crystals of $CeMn_{1-x}Sb_2$ are ground into powders and their powder x-ray diffraction pattern is collected at room temperature. The pattern, shown in Fig. 2, affirms the presence of flux Bi and an alien phase MnSb. Two unknown minor impurity peaks located at 22.45° and 25.44° are also found.

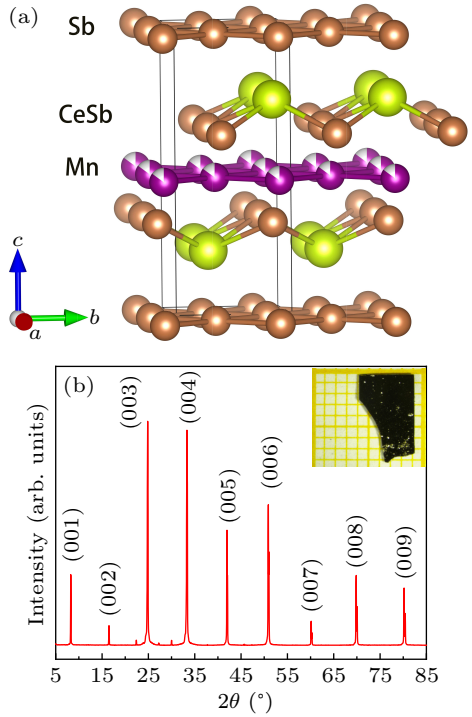


Fig. 1. (a) Crystal structures of $CeMn_{0.85}Sb_2$ obtained from the single crystal refinements. The green, brown, and purple balls stand for Ce, Sb, and Mn, respectively. (b) A typical out-of-plane x-ray diffraction pattern of the obtained samples. Unindexed diffraction peaks between 20°–30° are from Bi flux and MnSb impurity. The inset is a photograph of the crystal.

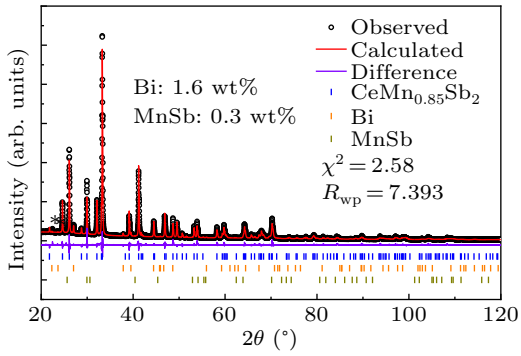


Fig. 2. Room-temperature powder x-ray diffraction patterns for powdered single crystals of $CeMn_{0.85}Sb_2$. The Bi with a weight percent of 1.6% and MnSb with a weight percent of 0.3% are detected. Two unknown minor impurity peaks located at 22.45° and 25.44° are marked with asterisks.

3.2. Magnetism

Figure 3(a) shows the temperature-dependent magnetizations, $M(T)$, of $CeMn_{0.85}Sb_2$ measured with magnetic fields parallel to the *c*-axis ($H \parallel c$). The FC curves overlap the ZFC curves over the measured range. The $M(T)$ curve measured with $H = 5$ kOe shows a broad peak at ~ 160 K (defined as the Néel temperature, T_N), indicating an AFM order, possibly for the Mn sublattice. This order temperature is comparable to 175 K and 170 K reported for Mn-sublattice in the $PrMn_{0.81}Sb_2$ and $NdMn_{0.88}Sb_2$, respectively.[28,30] But it is somewhat higher than that reported by Sologub *et al.* (~ 130 K).[31] With increasing H, the peak shifts toward lower temperature and decreases from ~ 160 K ($H = 5$ kOe) to ~ 130 K ($H = 70$ kOe) as shown in Fig. 3(a). There is no additional sign of magnetic order for Ce-sublattice at low temperatures.

Isothermal magnetizations, $M(H)$, of $CeMn_{0.85}Sb_2$ measured at different temperatures with $H \parallel c$ are shown in Fig. 3(b). All these $M(H)$ curves measured at 300 K, 30 K, and 2 K deviate from linearity around the zero magnetic field region and can be regarded as a straight line superposed with an FM component (see the inset in Fig. 3(b)). The FM components for the 300 K $M(H)$ curve saturate with a saturation magnetization (M_s) of ~ 0.05 μ_B/f.u. This small FM component is more likely due to the impurity phase MnSb because even the $M(H)$ curve measured at 300 K (much above the T_N) has this FM component. MnSb has an FM transition at ~ 590 K.[46] It should be noted that a similar superposition of small FM components in the $M(H)$ curves measured above magnetic transition temperatures has been observed in other $AMn_{1-\delta}Sb_2$ (A = La, Pr, Nd) compounds.[28,30]

When H is perpendicular to the *c*-axis ($H \perp c$), $M(T)$ curves measured with different H are plotted in Fig. 3(c). The $M(T)$ curve measured with 5 kOe does not show the AFM peak as in the case of $H \parallel c$ but displays a slope change around the T_N (see the inset in Fig. 3(c)), indicating the magnetic order of Mn-sublattice. With further cooling, there is another slope change around ~ 116 K, indicating a possible spin reorientation of the Mn sublattice. The kinks around 116 K are suppressed toward lower temperatures and disappear when H is 30 kOe or larger. The $M(T)$ curves measured with 30 kOe and 50 kOe show ferro- or ferrimagnetic-like behavior, indicating a field-induced magnetic state change for Mn-sublattice.

To further understand these magnetic transitions, isothermal $M(H)$ curves of $CeMn_{0.85}Sb_2$ measured with $H \perp c$ at different temperatures are shown in Fig. 3(d). The curve measured at 300 K is similar to the $H \parallel c$ case and shows linear behavior superposed with an FM component, agreeing well with the presence of a tiny amount of FM impurity MnSb in the sample. At 80 K, M increases with H and tends to saturate after H is 30 kOe or larger, indicating the presence of an

FM component with $M_s = 1.81$ μ_B/f.u. At 30 K, M increases linearly first, then shows a sharp increase at 19.6 kOe (determined by the dM/dH), indicating a field-induced spin-flop transition. M tends to saturate when H is larger than 20 kOe, and M_s is about 2.44 μ_B/f.u. The ferromagnetic components at 80 K and 30 K are too large to be explained by the tiny amount of FM MnSb impurity, and they are possible due to a field-induced canting of Mn moments. In the $AMnX_2$ family, the Mn moments are generally parallel to the c-axis (or perpendicular to the two-dimensional layers), examples are $YbMnBi_2$,[47] $YbMnSb_2$,[48] $PrMn_{0.81}Sb_2$,[28] $EuMnSb_2$,[49] and $LaMn_{0.91}Sb_2$.[30] When applied magnetic fields are perpendicular to the c-axis, they would tend to align the Mn moments toward the magnetic field direction, resulting in canted Mn moments. At 2 K, the $M(H)$ curves at 2 K show saturation with a M_s of 2.68 μ_B/f.u. and a large hysteresis with a coercivity of 6 kOe. The origin of coercivity is not generally understood. In comparison with $LaMn_{0.91}Sb_2$ which also shows saturation without hysteresis in the $M(H)$ curves at 2 K,[30] the presence of the coercivity in $CeMn_{0.85}Sb_2$ may be related to the magnetocrystalline anisotropy induced by the rare earth element Ce.[50] The Ce-sublattice shows spin glass behavior (vide infra) and can be responsible for the observed coercivity.[51]

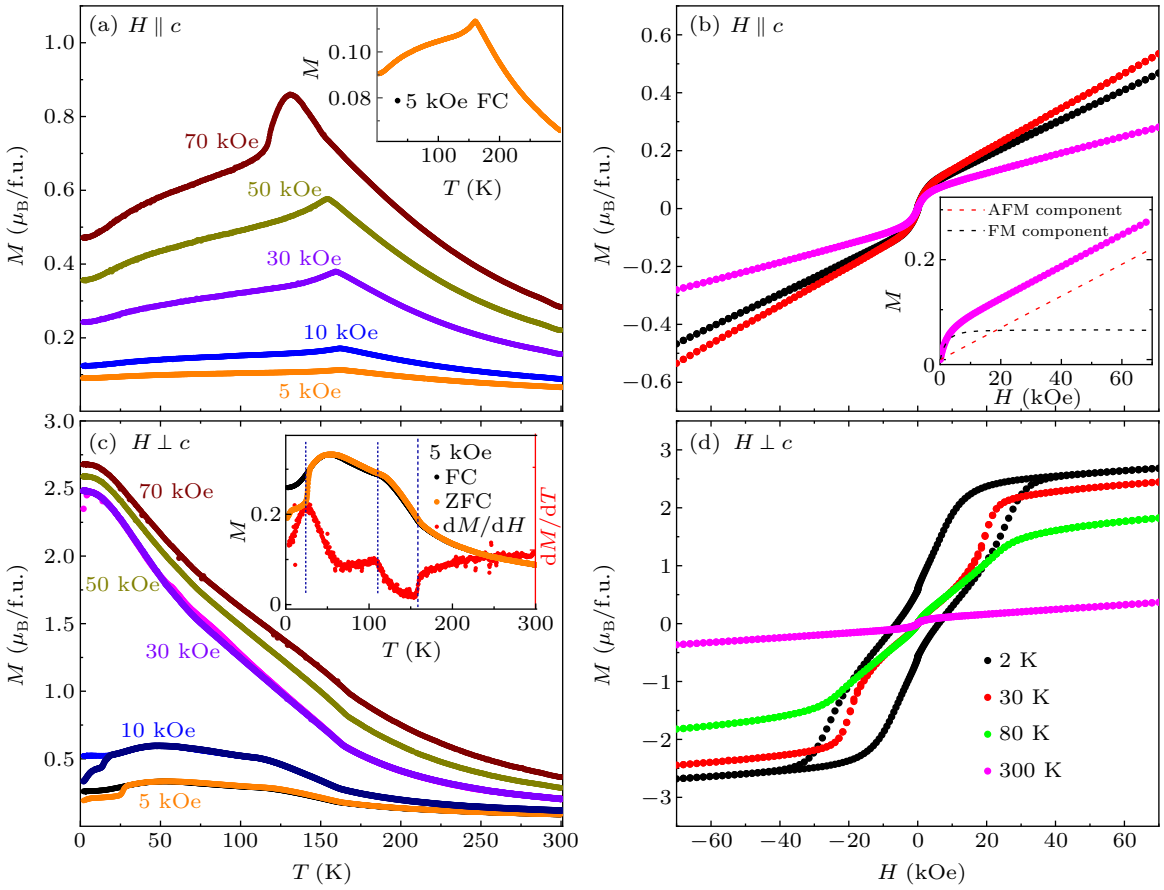


Fig. 3. (a) Temperature-dependent magnetizations of $CeMn_{0.85}Sb_2$ measured with $H \parallel c$. The inset shows the enlarged view for $H = 5$ kOe curves. (b) Isothermal magnetizations of $CeMn_{0.85}Sb_2$ measured with $H \parallel c$. The inset shows the decomposition of the AFM and FM components for the 300 K data. (c) Temperature-dependent magnetizations of $CeMn_{0.85}Sb_2$ measured with $H \perp c$. The inset shows an enlarged view for $H = 5$ kOe curves and the corresponding dM/dH for the FC curve. (d) Isothermal magnetizations of $CeMn_{0.85}Sb_2$ measured with $H \perp c$.

In the case of $H \perp c$, there is also no sign of magnetic order of Ce-sublattice at low temperatures. But we see a divergence of ZFC and FC curves below 18 K (see the inset of Fig. 3(c)). To further study this anomaly, we carry out AC magnetic susceptibility measurements at low temperatures. The temperature-dependent AC susceptibility data measured at different frequencies are shown in Fig. 4. A shift of peak positions toward higher temperatures (from 15.3 K to 18.3 K) with increasing frequency is observed. The peaks in AC susceptibility increase with the increase of frequency, indicating either a glassy or a superparamagnetic state. We plot the peak temperature (T_{sg}) vs. the logarithmic frequency $\log(f)$ in Fig. 4. According to the equation, $K = \Delta T_{sg}/(T_{sg}\Delta\log(f))$, where ΔT_{sg} and $\Delta\log(f)$ refer to the difference of spin-glass transition temperature and logarithmic frequency between measurements at different frequencies. The fitting results in $K = 0.08$, which indicates a spin-glass system.[52,53]

To further study the magnetic transition of $CeMn_{0.85}Sb_2$, temperature-dependent specific heat, $C_p(T)$, of $CeMn_{0.85}Sb_2$ is shown in Fig. 5(a). A λ-type anomaly around 160 K

is observed, supporting the long-range AFM order of Mn-sublattice. This anomaly can be suppressed toward lower temperatures by applying H (see Fig. 5(b)), which is consistent with the shift of AFM peaks of $M(T)$ curves ($H \parallel c$). It should be noted that the single crystal was pulled away from the sample puck for the C_p measurement when H of 50 kOe was applied.

At low temperatures, there is no sign of magnetic order regarding the Ce-sublattice. The C_p between 2 K and 50 K was further measured with 0 kOe, 10 kOe, 20 kOe, and 30 kOe (see Fig. 5(c)). There is no sign of magnetic order and the $C_p(T)$ curves measured under different H are almost superimposed with each other, which is consistent with the spin-glass behavior. The inset of Fig. 5(c) shows the lowest part of C_p/T vs. T^2 and the data are fitted by an approximated Debye model, $C_p/T = \gamma + \beta T^2$. The fitting (the red dashed line) gives a Sommerfeld coefficient (γ) of 24.6 mJ·mol^{-1}·K^{-2}, which is smaller than some typical Ce-based compounds in this series, such as $CeNiSb_2$ (55 mJ·mol^{-1}·K^{-2}),[54] $CeAuSb_2$ (90 mJ·mol^{-1}·K^{-2}),[54] $CeAgSb_2$(75 mJ·mol^{-1}·K^{-2}),[55] and $CeCd_{0.7}Sb_2$ (77 mJ·mol^{-1}·K^{-2}).[24]

We further study the magnetic contribution from Ce for $CeMn_{0.85}Sb_2$ by subtracting its nonmagnetic analog $LaMn_{0.91}Sb_2$ (normalized at 200 K) as its phonon contributions. The resulting C_m/T vs. T curve is shown in Fig. 5(d). Except for the peak around 160 K, there is a broad peak at lower temperatures which may be due to the crystalline field effect. The integrated entropy up to 150 K (below the T_N for the Mn-sublattice) is about 13.2 J·mol^{-1}·K^{-1}, which is not far from the theoretical value of 14.9 J·mol^{-1}·K^{-1} for a Ce^{3+} ($J = 5/2$).

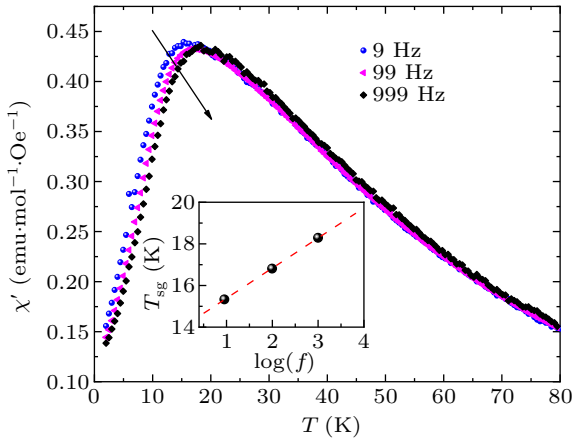


Fig. 4. The AC susceptibility data of $CeMn_{0.85}Sb_2$ measured with $H \perp c$ with different frequencies. The inset shows the peak temperature (T_{sg}) vs. the logarithmic frequency $\log(f)$.

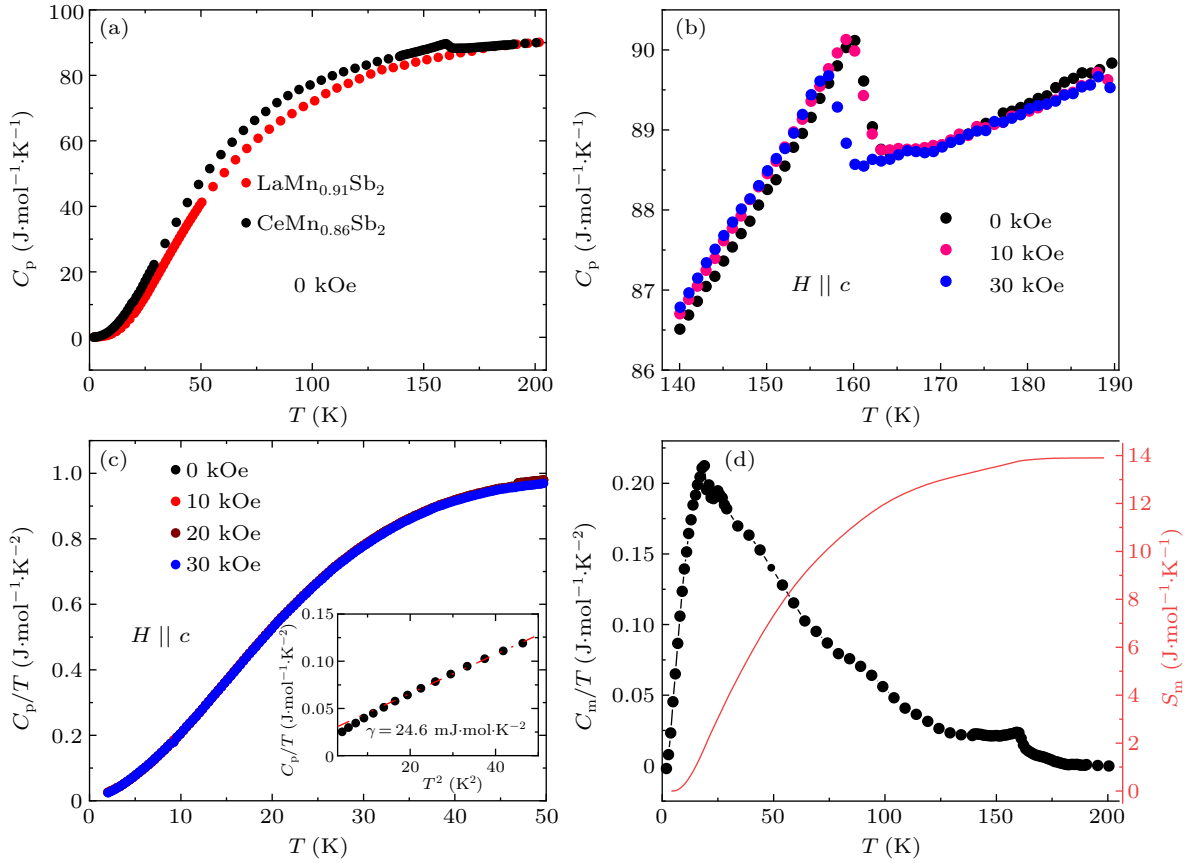


Fig. 5. (a) Temperature-dependent specific heat capacity $C_p(T)$ for $CeMn_{0.85}Sb_2$ and its non-magnetic analog $LaMn_{0.91}Sb_2$ (normalized according to 200 K data). (b) The $C_p(T)$ curves measured between 140 K and 190 K with $H = 0$ kOe, 10 kOe, and 30 kOe. (c) The C_p/T vs. T curves, measured under $H = 0$ kOe, 10 kOe, 20 kOe, and 30 kOe, below 50 K. The inset shows the Debye model fitting in the lowest temperature range. (d) The magnetic contributions of heat capacity C_m/T vs. T and the corresponding entropy.

3.3. Electrical resistivity

Temperature-dependent resistivities of $CeMn_{0.85}Sb_2$ were measured with electrical current parallel to the c-axis (ρ_c) and the ab-plane (ρ_{ab}), respectively, are shown in Fig. 6(a). Metallic behaviors are observed in both directions. There is no Kondo behavior and no corresponding anomaly related to the magnetic transition. The ρ_c/ρ_{ab} ratio is about 14 at 300 K and about 9.5 at 2 K, suggesting a quasi-2D electronic band structure and is consistent with the layered crystal structure of $CeMn_{0.85}Sb_2$. The residual resistivity ratios are 2 and 1.6 for ρ_c and ρ_{ab}, respectively. The resistivity of ρ_{ab} measured under 90 kOe is almost coincident with 0 kOe for temperatures higher than 75 K and shows a small negative magnetoresistance at low temperatures (about -4% at 2 K). The small negative magnetoresistance may be attributed to the suppression of the magnetic scattering.

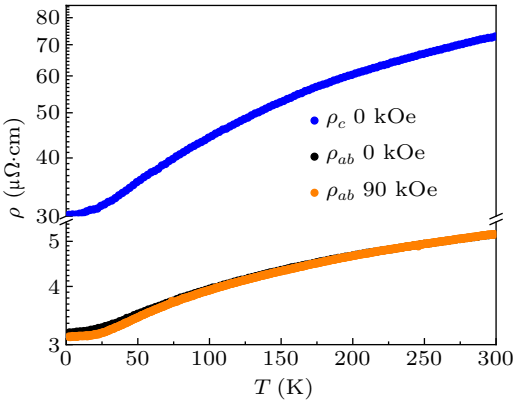


Fig. 6. Temperature-dependent resistivity with electrical current parallel to the c-axis (ρ_c) and the ab-plane (ρ_{ab}).

4. Conclusion

Single crystals of $CeMn_{0.85}Sb_2$ have been successfully synthesized by using Bi as the flux. Analysis of SCXRD data confirms that $CeMn_{0.85}Sb_2$ crystallizes in the $HfCuSi_2$-type tetragonal structure with the space group $P4/nmm$ (No. 129). Our magnetic susceptibility and specific heat measurements confirm a long-range AFM order for $CeMn_{0.85}Sb_2$ with a T_N of ~ 160 K. In the case of $H \parallel c$, the intrinsic $M(H)$ curves (below T_N) display linear behavior without hysteresis, consistent with AFM order of Mn-sublattices. However, the $M(H)$ curves measured below T_N with $H \perp c$ show saturation and even large hysteresis, indicating the presence of the FM component. The FM component is possibly due to the canting of Mn-spins in the ab-plane. In addition, a field-induced spin-flop transition is observed in the case of $H \perp c$, indicating a field-induced spin reorientation of Mn spins. In $CeMn_{0.85}Sb_2$, there is no indication of magnetic order for Ce-sublattice down to 2 K. However, there is a spin glass behavior below 18 K in the case of $H \perp c$, which may correspond to the Ce-sublattice. Electrical resistivity measurements indicate metallic behavior with large anisotropy, supporting its quasi-two-dimensional layered crystal structure.

Acknowledgments

HLF thanks professor Peijie Sun for insightful discussions. Project supported by the National Natural Science Foundation of China (Grant Nos. U22A6005, U2032204, and 12104492), the Guangdong Major Scientific Research Project (Grant No. 2018KZDXM061), the National Key Research and Development Program of China (Grant No. 2021YFA1400401), the Strategic Priority Research Program of the Chinese Academy of Sciences (Grant No. XDB33010000), the K. C. Wong Education Foundation (Grant No. GJTD-2018-01), and the Informatization Plan of Chinese Academy of Sciences (Grant No. CAS-WX2021SF-0102).

References

[1] Zhang A M, Liu C L, Yi C J, Zhao G H, Xia T L, Shi Y G, Yu R, Wang X Q, Chen C F and Zhang Q M 2016 *Nat. Commun.* **7** 13833
[2] Qiu Z Y, Le C C, Dai Y M, Xu B, He J B, Yang R, Chen G F, Hu J P and Qiu X G 2018 *Phys. Rev. B* **98** 115151
[3] He B J, Fu Y, Zhao L X, Liang H, Chen D, Leng Y M, Wang X M, Li J, Zhang S, Xue M Q, Li C H, Zhang P, Ren Z A and Chen G F 2017 *Phys. Rev. B* **95** 045128
[4] Wang K F, Graf D, Wang L M, Lei H C, Tozer S W and Petrovic C 2012 *Phys. Rev. B* **85** 041101
[5] Feng Y, Wang Z J, Chen C Y, Shi Y G, Xie Z J, Yi H M, Liang A J, He S L, He J F, Peng Y Y, Liu X, Liu Y, Zhao L, Liu G D, Dong X L, Zhang J, Chen C T, Xu Z Y, Dai X, Fang Z and Zhou X J 2014 *Sci. Rep.* **4** 5385
[6] You J S, Lee I, Choi E S, Joe Y J, Shim J H and Kim J S 2019 *Curr. Appl. Phys.* **19** 230
[7] Liu Y, Ma T, Zhou L, Straszheim W E, Islam F, Jensen B A, Tian W, Heitmann T, Rosenberg R A, Wilde J M, Li B, Kreyssig A, Goldman A I, Ueland B G, McQueeney R J and Vaknin D 2019 *Phys. Rev. B* **99** 054435
[8] Wang Y Y, Xu S, Sun L L and Xia T L 2018 *Phys. Rev. Mater.* **2** 021201
[9] Pan Y, Fan F R, Hong X C, He B, Le C C, Schnelle W, He Y K, Imasato K, Borrmann H, Hess C, Büchner B, Sun Y, Fu C G, Snyder G J and Felser C 2021 *Adv. Mater.* **33** 2003168
[10] Borisenko S, Evtushinsky D, Gibson Q, Yaresko A, Koepernik K, Kim T, Ali M, van der Brink J, Hoesch M, Fedorov A, Haubold E, Kushnirenko Y, Soldatov I, Schäfer R and Cava R J 2019 *Nat. Commun.* **10** 3424
[11] Pan Y, Le C C, He B, Watzman S J, Yao M Y, Gooth J, Heremans J P, Sun Y and Felser C 2022 *Nat. Mater.* **21** 203
[12] Masuda H, Sakai H, Tokunaga M, Yamasaki Y C, Miyake A, Shiogai J, Nakamura S, Awaji S, Tsukazaki A, Nakao H, Murakami Y, Arima T, Tokura Y and Ishwata S 2016 *Sci. Adv.* **2** e1501117
[13] Sun Z L, Wang H H, Wang A F, Lei B, Zhuo W Z, Yu F H, Zhou X Y, Ying J J, Xiang Z J, Wu T and Chen X H 2022 *Adv. Funct. Mater.* **32** 2202188
[14] Zhang L Y, Sun Z L, Wang A F, Xia Y Y, Mi X R, Zhang L, He M Q, Chai Y S, Wu T, Wang R, Zhou X Y and Chen X H 2021 *Phys. Rev. B* **104** 205108
[15] Park J, Lee G, Wolff-Fabris F, Koh Y Y, Eom M J, Kim Y K, Farhan M A, Jo Y J, Kim C, Shim J H and Kim J S 2011 *Phys. Rev. Lett.* **107** 126402

[16] Liu J Y, Hu J, Cao H B, Zhu Y L, Chuang A, Graf D, Adams J A, Radmanesh S M A, Spinu L, Choirescu I and Mao Z Q 2016 *Sci. Rep.* **6** 30525

[17] Klemenz S, Lei S M and Schoop L M 2019 *Annu. Rev. Mater. Sci.* **49** 185

[18] Guo Y F, Princep A J, Zhang X, Manuel P, Khalyavin D, Mazin I I, Shi Y G and Boothroyd A T 2014 *Phys. Rev. B* **90** 075120

[19] Stockert O, Arndt J, Faulhaber E, Geibel C, Jeevan H S, Kirchner S, Loewenhaupt M, Schmalzl K, Schmidt W, Si Q and Steglich F 2011 *Nat. Phys.* **7** 119

[20] Weng Z F, Smidman M, Jiao L, Lu X and Yuan H Q 2016 *Rep. Prog. Phys.* **79** 094503

[21] Shen B, Zhang Y J, Komijani Y, Nicklas M, Borth R, Wang A, Chen Y, Nie Z Y, Li R, Lu X, Lee H, Smidman M, Steglich F, Coleman P and Yuan H Q 2020 *Nature* **579** 51

[22] Balicas L, Nakatsuji S, Lee H, Schlottmann P, Murphy T P and Fisk Z 2005 *Phys. Rev. B* **72** 064422

[23] Thomas S M, Rosa P F S, Lee S B, Parameswaran S A, Fisk Z and Xia J 2016 *Phys. Rev. B* **93** 075149

[24] Rosa P F S, Bourg R J, Jesus B R, Pagliuso P G and Fisk Z 2015 *Phys. Rev. B* **92** 134421

[25] Wang Y Y, Yu Q H and Xia T L 2016 *Chin. Phys. B* **25** 107503

[26] He J B, Fu Y, Zhao L X, Liang H, Chen D, Leng Y M, Wang X M, Li J, Zhang S, Xue M Q, Li C H, Zhang P, Ren Z A and Chen G F 2017 *Phys. Rev. B* **95** 045128

[27] Huang S L, Kim J S, Shelton W A and Jin R Y 2017 *Proc. Natl. Acad. Sci.* **114** 6256

[28] Takahashi Y, Urata T and Ikuta H 2021 *Phys. Rev. B* **104** 054408

[29] Soh J R, Manuel P, Schröter N M B, Yi C J, Orlandi F, Shi Y G, Prabhakaran D and Boothroyd A T 2019 *Phys. Rev. B* **100** 174406

[30] Li Y, Yang M, Yan D Y, Miao S S, Yang H X, Feng H L and Shi Y G 2022 *Phys. Rev. B* **105** 224429

[31] Guo Y F, Princep A J, Zhang X, *et al.* 2014 *Phys. Rev. B* **90** 075120

[32] Zhang A, Liu C, Yi C, *et al.* 2016 *Nat. Commun.* **7** 13833

[33] Sapkota A, Classen L, Stone MB, *et al.* 2020 *Phys. Rev. B* **101** 041111

[34] Masuda H, Sakai H, Tokunaga M, *et al.* 2016 *Sci. Adv.* **2** e1501117

[35] Sologub O, Hiebl K, Rogl P and Bodak O 1995 *J. Alloys Compd.* **227** 40

[36] Sheldrick G M and Schneider T R 1997 *Meth. Enzymol.* **277** 319

[37] Sheldrick G M 2008 *Acta Crystal. Sec. A* **64** 112

[38] Toby B H and Von Dreele R B 2013 *J. Appl. Cryst.* **46** 544

[39] Wang A, Zaliznyak I, Ren W, Wu L, Graf D, Garlea V O, Warren J B, Bozin E, Zhu Y and Petrovic C 2016 *Phys. Rev. B* **94** 165161

[40] See supplemental materials for details on crystallographic information files (Cif) for $CeMn_{0.85}Sb_2$

[41] Park T, Sidorov V A, Lee H, Fisk Z and Thompson J D 2005 *Phys. Rev. B* **72** 060410

[42] Adriano C, Rosa P F S, Jesus C B R, Grant T, Fisk Z, Garcia D J and Pagliuso P G 2015 *J. Appl. Phys.* **117** 17C103

[43] Rosa P F S, Jesus C B R, Adriano C, Fisk Z and Pagliuso P G 2015 *J. Phys.: Conf. Ser.* **592** 012063

[44] Seo S, Sidorov V A, Lee H, Jiang D, Fisk Z, Thompson J D and Park T 2012 *Phys. Rev. B* **85** 205145

[45] Baranets S and Bobev S 2021 *J. Solid State Chem.* **303** 122467

[46] Markandeyulu G and Rao R K V S 1987 *J. Magn. Magn. Mater.* **67** 215

[47] Soh J R, Jacobsen H, Ouladdiaf B, Ivanov A, Piovano A, Tejsner T, Feng Z, Wang H, Guo Y, Shi Y and Boothroyd 2019 *Phys. Rev. B* **100** 144431

[48] Soh J R, Tobin S M, Su H, Zivkovic I, Ouladdiaf B, Stunault A, Rodríguez-Velamazán A, Beauvois K, Guo Y and Boothroyd A T 2021 *Phys. Rev. B* **104** L161103

[49] Gong D, Huang S, Ye F, Gui X, Zhang J, Xie W and Jin R Y 2020 *Phys. Rev. B* **101** 224422

[50] Hirosawa S, Nishino M and Miyashita S 2017 *Adv. Nat. Sci: Nanosci. Nanotechnol.* **8** 013002

[51] Monod P, Prejean J J and Tissier B 2008 *J. Appl. Phys.* **50** 7324

[52] Mydosh J A 1993 *Spin Glasses: An Experimental Introduction* (1st edn.) (Boca Raton: CRC Press)

[53] Harikishnan S, Naveen Kumar C M, Bhat H L, *et al.* 2008 *J. Phys.: Condens. Matter* **20** 275234

[54] Thamizhavel A, Takeuchi T, Okubo T, Yamada M, Asai R, Kirita S, Galatanu A, Yamamoto E, Ebihara T, Inada Y, Settai R and Ōnuki Y 2003 *Phys. Rev. B* **68** 054427

[55] Muro Y, Takeda N and Ishkawa M 1997 *J. Alloys Compd.* **257** 23